Physical Communication 5 (2012) 289–295

Contents lists available at SciVerse ScienceDirect

Physical Communication

journal homepage: www.elsevier.com/locate/phycom

Full length article

The effect of polarization separation on the performance of Candecomp/Parafac-based vector sensor array processing

Xijing Guo [a,b], Sebastian Miron [a,*], David Brie [a]

[a] Centre de Recherche en Automatique de Nancy (CRAN), Nancy-Université, CNRS, Boulevard des Aiguillettes, B.P. 239, F-54506 Vandœuvre-lès-Nancy, France

[b] Department of Information and Communication Engineering, Xi'an Jiaotong University, 710049 Xi'an, China

ARTICLE INFO

Article history:
Received 9 December 2011
Received in revised form 13 January 2012
Accepted 1 February 2012
Available online 8 February 2012

Keywords:
Polarization separation
Vector sensor array
Candecomp/Parafac

ABSTRACT

In this paper we generalize the *polarization separation* measure introduced by Compton (1981) [2] for collocated sources, to the case of two sources with distinct DOAs recorded on a vector sensor array. We give a geometrical interpretation of this new measure and show that this polarization separation becomes essential for source estimation accuracy when the angular separation is insufficient.

1. Introduction

In the context of extensively desired high data transmission rate and reliability in wireless communication systems, the *polarization diversity* is getting more and more attention in the literature. Fourth-generation (4G) systems are expected to support data rates of the order of 100 Mb/s in the outdoor environment and 1 Gb/s in the indoor/stationary environment [1]. In order to support such large payloads, the physical layer must provide a much more efficient use of electromagnetic field properties such as its polarization. To fully exploit this property of the electromagnetic waves, polarization sensitive antennas are used both at the transmitter and receiver.

In [2,3] the performances of arrays consisting of two/three mutually perpendicular dipoles are investigated and a *polarization separation* for spatially collocated sources, based on Poincaré sphere [4], is proposed. Nehorai and Paldi introduced in [5] a signal model for a vector sensor comprising a spatially collocated but diversely oriented collection of three electrically short dipoles and three magnetically small loops. A variety of Direction Of Arrival (DOA) finding, polarization estimation and tracking schemes, using these collocated vector sensors, were proposed in [6–14] and performance bounds for vector sensor arrays were derived in [5,6,15,16].

However, to the best of our knowledge the influence of polarization separation between two spatially non-collocated sources on source estimation algorithms has not been yet investigated. In this paper we introduce a novel measure for the *polarization separation* between two sources having *distinct DOAs*, that generalizes the source separation definition for collocated sources presented in [2]. We provide a geometrical interpretation of this new quantity and analyze its influence on source estimation accuracy, using an algorithm based on a Candecomp/Parafac representation of the vector sensor array. Due to its nice identifiability properties (see [12,14]), this Candecomp/Parafac scheme allows to jointly and uniquely estimate the DOAs, polarizations and time signals of the impinging sources, from the recorded data. This makes the Candecomp/Parafac model very attractive for digital communications applications such as satellite or wireless communications. Nevertheless, the scope of the results presented in this paper is not limited to the Candecomp/Parafac model and can be extended to any vector sensor array scheme.

* Corresponding author.
E-mail address: sebastian.miron@cran.uhp-nancy.fr (S. Miron).

1874-4907/$ – see front matter © 2012 Elsevier B.V. All rights reserved.
doi:10.1016/j.phycom.2012.02.002

The remainder of this paper is organized as follows. In Section 2 we present the Candecomp/Parafac model of the data recorded on a vector sensor array. Section 3 introduces the polarization separation between two spatially non-collocated sources and provides a geometrical interpretation for it. Section 4 illustrates this novel quantity in numerical simulations and final remarks are given in Section 5.

2. The Candecomp/Parafac model of the vector sensor array data

In this section we present the Candecomp/Parafac model for polarized sources recorded on a vector sensor array. Consider an array of M displaced but otherwise identical electromagnetic (EM) sensors, collecting L narrowband temporal signal samples emitted by K (known *a priori*) spatially distinct far-field sources. For the kth incoming wave, its DOA can be totally determined by the azimuth angle $\phi_k \in [0, \pi)$ (measured from $+x$-axis) and the elevation angle $\psi_k \in [-\pi/2, \pi/2]$ (measured from the ground), as shown in Fig. 1. A 2×1 complex vector

$$\mathbf{g}_k \triangleq \mathbf{g}(\alpha_k, \beta_k) = \begin{bmatrix} g_\phi(\alpha_k, \beta_k) \\ g_\psi(\alpha_k, \beta_k) \end{bmatrix} = \begin{bmatrix} \cos\alpha_k & \sin\alpha_k \\ -\sin\alpha_k & \cos\alpha_k \end{bmatrix} \begin{bmatrix} \cos\beta_k \\ j\sin\beta_k \end{bmatrix} \tag{1}$$

is used to depict the polarization state of the kth signal in terms of the orientation angle $\alpha_k \in (-\pi/2, \pi/2]$ and the ellipticity angle $\beta_k \in [-\pi/4, \pi/4]$.

For one EM vector sensor, if the incoming wave has unit power, the electric- and magnetic-field measurements in Cartesian coordinates, $\mathbf{e}(\phi_k, \psi_k, \alpha_k, \beta_k) \triangleq [e_x^{(k)}, e_y^{(k)}, e_z^{(k)}]^T$ and $\mathbf{h}(\phi_k, \psi_k, \alpha_k, \beta_k) \triangleq [h_x^{(k)}, h_y^{(k)}, h_z^{(k)}]^T$, can be stacked up in a 6×1 vector $\mathbf{b}_k$ (see also [5]), that will be referred to as *polarization vector*, as it follows

$$\mathbf{b}_k \triangleq \begin{bmatrix} \mathbf{e}(\phi_k, \psi_k, \alpha_k, \beta_k) \\ \mathbf{h}(\phi_k, \psi_k, \alpha_k, \beta_k) \end{bmatrix} = \underbrace{\begin{bmatrix} -\sin\phi_k & -\cos\phi_k\sin\psi_k \\ \cos\phi_k & -\sin\phi_k\sin\psi_k \\ 0 & \cos\psi_k \\ -\cos\phi_k\sin\psi_k & \sin\phi_k \\ -\sin\phi_k\sin\psi_k & -\cos\phi_k \\ \cos\psi_k & 0 \end{bmatrix}}_{\mathbf{F}(\phi_k, \psi_k)} \mathbf{g}_k. \tag{2}$$

The 6×2 matrix $\mathbf{F}_k \triangleq \mathbf{F}(\phi_k, \psi_k)$ is the *steering matrix* [17] and it characterizes the capacity of a vector sensor to convert the information carried on an impinging polarized plane wave defined in polar coordinates, into the six electromagnetic-field-associated electric signals in the corresponding Cartesian coordinates. Thus, the 6×1 complex vector $\mathbf{b}_k = \mathbf{F}(\phi_k, \psi_k)\mathbf{g}(\alpha_k, \beta_k)$ models the response of a vector sensor to the kth polarized source.

Denoting by $\{\mathbf{r}_m\}_{m=1}^M$, the coordinates vectors of the M vector sensors in the reference frame and by $\mathbf{u}(\phi, \psi) = [\cos\phi\cos\psi \quad \sin\phi\cos\psi \quad \sin\psi]^T$ the unit vector in the source direction, the phase shifts induced by the displacements of the mth ($m = 1, \ldots, M$) vector sensor relative to the reference one is then given by $a_m(\phi, \psi) = \exp\left\{j2\pi \mathbf{r}_m^T \mathbf{u}(\phi, \psi)/\lambda\right\}$, where λ is the wavelength.

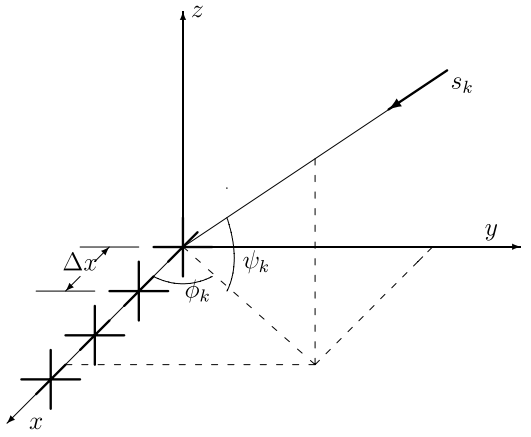

Fig. 1. The vector sensor array: acquisition scheme.

Define $\mathbf{a}(\phi, \psi) = [a_1(\phi, \psi), \ldots, a_M(\phi, \psi)]^T$, the steering vector of a virtual scalar sensor array having the same sensor configuration as the vector sensor array and let $\mathbf{S} \triangleq [\mathbf{s}_1, \ldots, \mathbf{s}_K]$ be a $L \times K$ matrix containing on its columns the L time samples for the K sources. Also, let us organize the L output snapshots of the vector sensor array in a $6M \times L$ matrix $\mathbf{Y} = [\mathbf{y}(t_1), \ldots, \mathbf{y}(t_L)]$, each column $\mathbf{y}(t_l)$ containing the recorded samples at time t_l on the 6 components of the M sensors. Denote by $\mathbf{A} \triangleq [\mathbf{a}_1(\phi_1, \psi_1), \ldots, \mathbf{a}_K(\phi_K, \psi_K)]$ the $M \times K$ matrix whose columns are the steering vectors of the K sources and by and $\mathbf{B} \triangleq [\mathbf{b}_1(\phi_1, \psi_1, \alpha_1, \beta_1), \ldots, \mathbf{b}_K(\phi_K, \psi_K, \alpha_K, \beta_K)]$ the $6 \times K$ matrix containing the polarization vectors of the sources. With these notations it can be shown that (see [12,14] for more details) $\mathbf{Y}$ can be expressed as

$$\mathbf{Y} = \begin{bmatrix} \mathbf{B}\mathbf{D}_1(\mathbf{A}) \\ \vdots \\ \mathbf{B}\mathbf{D}_M(\mathbf{A}) \end{bmatrix} \mathbf{S}^T + \mathbf{N} = (\mathbf{A} \odot \mathbf{B})\mathbf{S}^T + \mathbf{N} \tag{3}$$

where $\mathbf{D}_m(\mathbf{A}) = \mathrm{diag}\,(a_{m1}, \ldots, a_{mK})$ denotes the diagonal matrix with the mth row of $\mathbf{A}$ as its diagonal. Eq. (3) clearly expresses a Candecomp/Parafac model of the recorded data, with $\mathbf{N}$ a $6M \times K$ matrix modeling the additive noise on the vector sensor components and "$\odot$" the Khatri–Rao (Kronecker column-wise) product of two matrices.

3. Polarization separation between two sources on a vector sensor array

When performing the Candecomp/Parafac decomposition of the data, the estimation performance is mainly determined by the following three factors:

- the source correlation: the best performance is expected for uncorrelated sources
- the DOA angular separation: the algorithm performs better when the sources are not closely located
- the *polarization separation*.

While the source correlation and DOA angular separation are quite intuitive and well understood, it appears that role of polarization separation is not as obvious to apprehend. Indeed, viewed from the vector sensor array, the polarization signature of an incoming wave is given by its polarization vector $\mathbf{b}_k$, which depends on both polarization and DOA parameters.

In [3], the polarization separation based on Poincaré sphere [4] was introduced for collocated sources, *i.e.* sources having the same DOA. The main contribution of this paper is to extend the aforementioned polarization separation to the case of sources having distinct DOAs.

3.1. Derivation of the polarization separation for distinctly located sources

First of all, note that if the elevation angles of two sources are both equal to $\pm\pi/2$, their DOA's will overlap regardless of their azimuth angles. Adopt the definition suggested in [18] stating that the DOA's of two sources, denoted by (ϕ_1, ψ_1) and (ϕ_2, ψ_2), are *distinct* if

$$\begin{cases} (\phi_1, \psi_1) \neq (\phi_2, \psi_2), & \text{if } \psi_1 \neq \pm\pi/2; \\ \psi_1 \neq \psi_2, & \text{otherwise.} \end{cases} \tag{4}$$

Let $\Delta\phi \triangleq \phi_2 - \phi_1$ be the azimuth angle difference of the two sources. Denote by $\mathbf{b}_1$ and $\mathbf{b}_2$ the vectors representing the electromagnetic fields generated by the two polarized sources in Cartesian coordinates, as defined by (2). The inner product $\langle \mathbf{b}_1, \mathbf{b}_2 \rangle$ can then be related to the inner product between the two source polarization states by the equation

$$\langle \mathbf{b}_1, \mathbf{b}_2 \rangle = \langle \mathbf{g}_1, \mathbf{g}_2 \rangle_{\mathbf{F}_1^H \mathbf{F}_2} \triangleq \mathbf{g}_1^H \mathbf{F}_1^H \mathbf{F}_2 \mathbf{g}_2. \tag{5}$$

The 2×2 matrix $\mathbf{F}_1^H \mathbf{F}_2$ can be written as

$$\mathbf{F}_1^H \mathbf{F}_2 = \Sigma \begin{bmatrix} \cos\varepsilon & -\sin\varepsilon \\ \sin\varepsilon & \cos\varepsilon \end{bmatrix} \tag{6}$$

where

$$\Sigma = 1 + \sin\psi_1 \sin\psi_2 + \cos\psi_1 \cos\psi_2 \cos\Delta\phi \tag{7}$$

$$\varepsilon = \tan^{-1} \frac{(\sin\psi_1 + \sin\psi_2) \sin\Delta\phi}{\cos\psi_1 \cos\psi_2 + (1 + \sin\psi_1 \sin\psi_2) \cos\Delta\phi}. \tag{8}$$

See Appendix for the derivation.

In [3], the *polarization separation* was defined originally for two polarized sources with overlapping DOA's. We hereby extend it, by introducing the quantity $\Omega_\varepsilon \in [0, \pi]$ that satisfies

$$\cos\Omega_\varepsilon = \sin 2\beta_1 \sin 2\beta_2 + \cos 2\beta_1 \cos 2\beta_2 \cos 2(\alpha_2 - \alpha_1 + \varepsilon), \tag{9}$$

which generalizes the polarization separation to the case of sources having distinct DOA's. Thus we have

$$|\mathbf{b}_1^H \mathbf{b}_2| = |\mathbf{g}_1^H \mathbf{F}_1^H \mathbf{F}_2 \mathbf{g}_2| = \Sigma \sqrt{(1 + \cos\Omega_\varepsilon)/2}. \tag{10}$$

As ε vanishes, Ω_ε follows exactly the original definition on the polarization separation in [3], denoted by Ω_0. If $\varepsilon \neq 0$, by introducing this additional variable into α_2, the quantity Ω_ε coincides with the polarization separation between a pair of polarized sources having the same DOA and the polarization states given by (α_1, β_1) and $(\alpha_2 + \varepsilon, \beta_2)$ respectively. Thus, the polarization vectors of two sources are orthogonal only if the polarization separation $\Omega_\varepsilon = \pi$; the correlation, on the contrary, increases as Ω_ε tends to 0.

The relevance of the polarization separation as defined by (9) will be illustrated in Section 4.

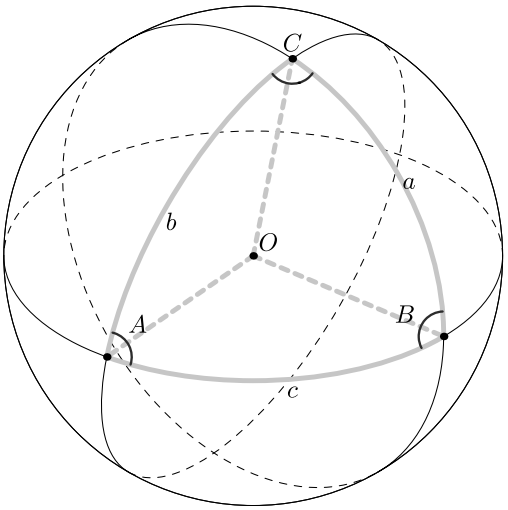

Fig. 2. The illustration of a spherical triangle.

3.2. Geometrical interpretation

We provide next a geometrical interpretation of the inner product (5) which is the basis of our definition for the polarization separation. To be self contained, we briefly review the main notions of spherical trigonometry; a thorough description can be found in many textbooks, *e.g.*, [19].

A spherical triangle *ABC* on the surface of a unit sphere is illustrated in Fig. 2. The three vertices are denoted by *A*, *B* and *C*, respectively while *O* denotes the center of the sphere. For notation simplicity we use the same notations for the dihedral angles at these vertices, *e.g.*, the dihedral angle at the vertex *A* between the plane *AOC* and the plane *AOB* is denoted by *A* as well. A *geodesic* is a part of an arc on a great circle of the sphere. Three such geodesics, respectively *a*, *b* and *c*, enclose the spherical triangle *ABC*. These quantities, are linked by the following identities [19] known respectively as the law of sines

$$\frac{\sin A}{\sin a} = \frac{\sin B}{\sin b} = \frac{\sin C}{\sin c} \tag{11}$$

and the law of cosines

$$\cos a = \cos b \cos c + \sin b \sin c \cos A \tag{12}$$

for the geodesic *a*; analogous cosine rules can be written for the other two geodesics *b* and *c*.

We now focus on the geometrical interpretation of the aforementioned inner product by considering two polarized sources with the DOA's defined by (ϕ_1, ψ_1) and

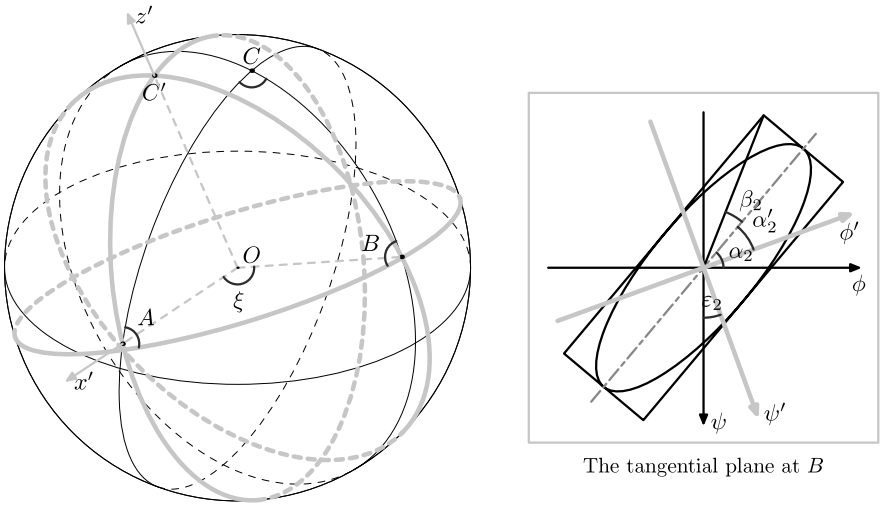

Fig. 3. The physical content of the factors that determine the DOA-dependent variables Σ and ε in (6). On the sphere, the geometrical representation of the DOA's of the signals is illustrated. The DOA's of the two sources, denoted by *A* and *B*, in both the original coordinate system and the rotated one afterward, indicated by the great circles of the gray color. The geometrical representation of the polarization state of the second signal is sketched in the tangential plane at *B*. Correspondingly, the gray axes are those after the coordinate rotation. β_2 is the ellipticity angle of the signal, which is invariant of the coordinate rotation. α_2 and α_2' are the orientation angles in the original and new coordinate systems respectively, which are related to the coordinate axis rotation ε_2 by $\alpha_2' = \alpha_2 - \varepsilon_2$.

(ϕ_2, ψ_2). We designate, for instance, *A* and *B* to represent the corresponding DOA's of the signals on the unit sphere, if *C* denotes the north pole,[1] as shown in Fig. 3.

We may appropriately rotate the coordinate system such that, in the new coordinate system, the DOA's of the two impinging waves both lie in the *x*–*y* plane. Following the procedures suggested in [17], this coordinate rotation is always possible. In Fig. 3, the gray curves on the sphere depict the new coordinate system, while the dark ones represent the original coordinate system and C' marks the north pole in the new coordinate system. According to the law of cosines, the angle between the two DOA's, or the *angular separation*, denoted by ξ, is intrinsically related to the DOA's by

$$\cos\xi = \sin\psi_1 \sin\psi_2 + \cos\psi_1 \cos\psi_2 \cos\Delta\phi. \tag{13}$$

Note that this angle also reflects the dihedral separation between the wavefronts of the two impinging waves. Thus the representations for the DOA's with respect to the new coordinate system are given by $(0, 0)$ and $(\xi, 0)$ respectively.

Observe in Fig. 3 the tangential plane to the DOA of one source. The coordinate rotation does not change the ellipticity angle of a polarized signal, only the orientation angle will be affected. From the perspective of the corresponding spherical coordinate system, it can be observed that the change is equal to the extent of the coordinate rotation over the orthogonal ϕ and ψ axes in the DOA tangential plane.

Next, we quantify the amount of changes on the orientation angles of the two polarization ellipses after rotation, denoted by ε_1 and ε_2. On the unit sphere, the geodesics that enclose the spherical triangle ABC' in the new coordinate system are measured up to $\pi/2, \pi/2$ and ξ, and the angles between each pair of them are also given by $\pi/2, \pi/2$ and ξ, respectively. In the original coordinate system, however, the bounding geodesics of the spherical triangle *ABC* are $(\pi/2 - \psi_1)$, $(\pi/2 - \psi_2)$ and ξ. The angles between these geodesic pairs, relative to their counterparts of the spherical triangle ABC' in the new coordinate system, are equal to $(\pi/2 - \varepsilon_1)$, $(\pi/2 + \varepsilon_2)$ and $\Delta\phi$. By the law of sines, we obtain

$$\frac{\cos\psi_1}{\cos\varepsilon_1} = \frac{\cos\psi_2}{\cos\varepsilon_2} = \frac{\sin\xi}{\sin\Delta\phi} \tag{14}$$

for the spherical triangle *ABC* from which the unknowns ε_1 and ε_2 can be determined.

The vector of electromagnetic components for the second source can be represented in the new coordinate system by

$$\begin{aligned}\mathbf{b}_2' &= \mathbf{F}(\xi, 0) \begin{bmatrix} \cos(\alpha_2 - \varepsilon_2) & -\sin(\alpha_2 - \varepsilon_2) \\ \sin(\alpha_2 - \varepsilon_2) & \cos(\alpha_2 - \varepsilon_2) \end{bmatrix} \begin{bmatrix} \cos\beta_2 \\ j\sin\beta_2 \end{bmatrix} \\ &= \mathbf{F}(\xi, 0) \underbrace{\begin{bmatrix} \cos\varepsilon_2 & -\sin\varepsilon_2 \\ \sin\varepsilon_2 & \cos\varepsilon_2 \end{bmatrix}}_{\mathbf{g}_2'} \mathbf{g}_2 . \end{aligned} \tag{15}$$

Analogously, for the first source, we get

$$\mathbf{b}_1' = \mathbf{F}(0, 0) \underbrace{\begin{bmatrix} \cos\varepsilon_1 & -\sin\varepsilon_1 \\ \sin\varepsilon_1 & \cos\varepsilon_1 \end{bmatrix}}_{\mathbf{g}_1'} \mathbf{g}_1 . \tag{16}$$

The inner product

$$\langle \mathbf{b}_1', \mathbf{b}_2' \rangle = \mathbf{g}_1^H \begin{bmatrix} \cos\varepsilon_1 & \sin\varepsilon_1 \\ -\sin\varepsilon_1 & \cos\varepsilon_1 \end{bmatrix}$$

[1] In spherical geometry, the north pole represents the intersection point of the unit sphere with the *z*-axis in the corresponding Cartesian coordinates system.

$$\times \underbrace{\begin{bmatrix} 1+\cos\xi & 0 \\ 0 & 1+\cos\xi \end{bmatrix}}_{\mathbf{F}(0,0)^H\mathbf{F}(\xi,0)} \times \begin{bmatrix} \cos\varepsilon_2 & -\sin\varepsilon_2 \\ \sin\varepsilon_2 & \cos\varepsilon_2 \end{bmatrix} \mathbf{g}_2 = \mathbf{g}_1^H \left(\Sigma \begin{bmatrix} \cos\varepsilon & -\sin\varepsilon \\ \sin\varepsilon & \cos\varepsilon \end{bmatrix} \right) \mathbf{g}_2 \quad (17)$$

is in accordance with (6), where $\Sigma = 1 + \cos\xi$ and $\varepsilon = \varepsilon_2 - \varepsilon_1$. This equality is natural since the inner product is constant with respect to any coordinate rotation.

4. Simulation results and discussion

In this section, some typical examples are designed to evaluate the influence of polarization separation on source estimation performance. To estimate the three matrices **A**, **B** and **S** from **Y**, we herein adopted the COMFAC algorithm proposed by Bro et al. in [20]. Each experiment uses $R = 500$ independent Monte Carlo runs. We suppose that the sources are uncorrelated and the noise Gaussian, temporally and spatially white. A uniform linear array (ULA) with an inter-sensor space of $\Delta x = \lambda/2$ is simulated. A number of $M = 13$ vector sensors and $L = 50$ snapshots and a SNR of 20 dB are used for all these simulations. The considered performance measure is the root mean square error (RMSE) of the source signals, given by

$$\text{RMSE} = \sqrt{\frac{1}{RLK} \sum_{r=1}^{R} \left\| \mathbf{S} - \hat{\mathbf{S}}_r \right\|_F^2}, \quad (18)$$

where $\hat{\mathbf{S}}_r$ is the estimate of **S** obtained in the rth trial. Once the Candecomp/Parafac decomposition is performed, a greedy least squares $(\hat{\mathbf{S}}_r, \mathbf{S})$-column matching algorithm [21] is applied to resolve the permutation ambiguities.

Example 1. This first example illustrates the role of polarization in source separation for two limit cases: identical/orthogonal polarizations. The results are shown in Fig. 4. Two polarized sources are considered, one source is nominated the reference source, and has a set of parameters fixed to $\phi_1 = 102.82°$, $\psi_1 = 11.57°$, $\alpha_1 = 35.81°$, and $\beta_1 = 32.94°$. The variable source, varies on ϕ_2, while $\psi_2 = \psi_1$. The polarization parameters for the second source were chosen such that $\mathbf{g}_1 = \mathbf{g}_2$ for the identical polarization case and $|\mathbf{g}_2^H \mathbf{g}_1| = 0$ for the orthogonal polarizations.

Comparing the curves of identically polarized sources with those of orthogonally polarized, one can see that polarization separation becomes an essential factor of source estimation performance if the angular separation between the two sources is small. As the two sources are getting closer to each other, $\varepsilon \to 0$ and consequently $\Sigma \to \Sigma_{\max} = 2$. From (10), $|\mathbf{b}_1^H \mathbf{b}_2| \approx 2\sqrt{(1+\cos\Omega_0)/2}$, which indicates that the polarization separations of the sources can completely determine the column inner-products of matrix **B**, and hence the performance of the separation method; otherwise, when the angular separation between sources is sufficient, this effect becomes negligible.

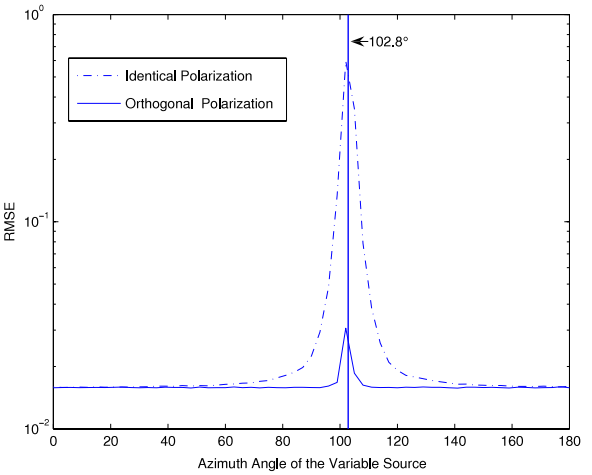

Fig. 4. The RMSE of source estimation versus their angular separation ($\psi_1 = \psi_2 = 11.6°$ varying ϕ_2).

Example 2. This example aims at investigating the effects of the polarization separation on the estimation of two sources from noise-corrupted data. The elevation angles $\psi_1 = \psi_2 = 0°$ are considered, resulting in $\varepsilon = 0$. This means that the polarization separation Ω_ε is independent from the source DOA's, according to (9). The azimuth angles are fixed to $\phi_1 = 90°$ for the reference source and the variable one deviates from it by ξ, that is $\phi_2 = \phi_1 + \xi$. Hence ξ is the source angular separation. Two sets of simulations are designed for some typical values of ξ, such as 0.03°, 0.3°, 0.6°, 1°, 2°, 4°, 8°, and 20°. Firstly, we assume that both sources are linearly polarized, *i.e.*, the ellipticity angles $\beta_1 = \beta_2 = 0$, and the orientation angles $\alpha_1 = 0°$ and α_2 varies from $-90°$ to 90°. Thus, the polarization separation Ω_ε is entirely defined by the orientation separation $\alpha_1 - \alpha_2$. It decreases from 180° to 0° (for $\alpha_2 = 0°$) and then increases up to $\Omega_\varepsilon = 180°$, for α_2 approaching 90°. The comparison is shown in Fig. 5(a). As expected, these RMSE curves are symmetric around $\alpha_2 = 0°$, presenting a homogeneous shape, which is accounted for by the variation pattern of the polarization separation. Then, we assume the reference source is characterized by the circular polarization with $\alpha_1 = 0$ and $\beta_1 = -45°$. The variable one has the same orientation angle while the ellipticity angle varies from $-45°$ to 45°. The simulation results for different values of ξ are shown in Fig. 5(b). In that case, the polarization separation is totally determined by the ellipticity separation $\beta_1 - \beta_2$. It grows monotonically from 0° to 180°.

These simulations reveal two key factors that directly affect the performance of polarized source estimation: the polarization separation and the angular separation; nevertheless, the extent of their effect varies. If the sources are inadequately separated in space ($\xi \leq 4°$ in our simulations), a slight increase in the polarization separation may cause a considerable gain on the source estimation performance, thus compensating the lack of angular separation. However, as the polarization separation exceeds some threshold value (around 40° in our case), its advantage fades and the RMSE reaches some minimum value

$$\Sigma = \sqrt{[\cos\psi_1 \cos\psi_2 + (1 + \sin\psi_1 \sin\psi_2)\cos\Delta\phi]^2 + (\sin\psi_1 + \sin\psi_2)^2 \sin^2\Delta\phi}. \quad \text{(A.4)}$$

Box I.

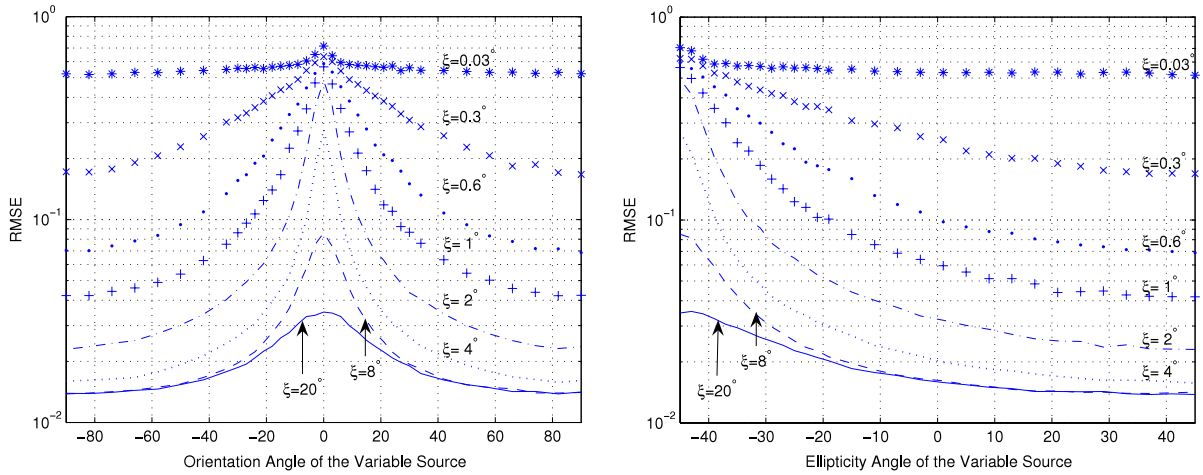

(a) $\beta_1 = \beta_2 = 0°, \alpha_1 = 90°$ varying α_2. (b) $\alpha_1 = \alpha_2 = 0°, \beta_1 = -45°$ varying β_2.

Fig. 5. The RMSE of source estimation versus their polarization separation.

representing the best achievable performance for a given angular separation. When the angular separation is large enough, it imposes the dominant effect. The polarization separation effect is then negligible. In the considered examples, this is the case when the sources are spatially separated by $\xi > 8°$ and the gain in raising either factor becomes insignificant: the best achievable performance is then mainly determined by the SNR. This result is illustrated in both plots on Fig. 5; the curves marked by $\xi = 8°$ and $\xi = 20°$ are tending to the same constant value.

5. Conclusions

In this paper we introduced a novel measure for polarization separation of two sources having distinct DOAs and provided a geometrical interpretation for it. Its importance on the source estimation performance was illustrated in numerical simulations. The simulations confirmed that polarization separation plays a key role in source estimation performance when the angular separation between the sources is insufficient. Meanwhile, when the spatial separation between the sources becomes significant the effect of the polarization separation vanishes.

Appendix. Derivation of Σ, ε and $\mathbf{F}_1^H\mathbf{F}_2$

Define a 2×2 matrix $\mathbf{W}$ such that

$$\mathbf{W} \triangleq \mathbf{F}_1^H\mathbf{F}_2 = \begin{bmatrix} W_{11} & W_{12} \\ W_{21} & W_{22} \end{bmatrix}. \quad \text{(A.1)}$$

If we denote $\Delta\phi \triangleq \phi_2 - \phi_1$, using definition (2) it can be shown that $\mathbf{W}$ is an antisymmetric matrix whose entries are given by

$$W_{11} = \cos\Delta\phi(\sin\psi_1 \sin\psi_2 + 1) + \cos\psi_1 \cos\psi_2 \quad \text{(A.2)}$$

$$W_{12} = -\sin\Delta\phi(\sin\psi_1 + \sin\psi_2) \quad \text{(A.3)}$$

and $W_{21} = -W_{12}, W_{22} = W_{11}$.

Let $\Sigma \triangleq \sqrt{W_{11}^2 + W_{12}^2}$, or Eq. (A.4) given in Box I. Observing that

$$\sin^2\Delta\phi = 1 - \cos^2\Delta\phi, \quad \text{(A.5)}$$

$$\cos^2\psi_1 \cos^2\psi_2 = 1 - \sin^2\psi_1 - \sin^2\psi_2 + \sin^2\psi_1 \sin^2\psi_2, \quad \text{(A.6)}$$

it can be simplified into

$$\Sigma = \sqrt{[1 + \sin\psi_1 \sin\psi_2 + \cos\psi_1 \cos\psi_2 \cos\Delta\phi]^2}. \quad \text{(A.7)}$$

If we denote $\Delta\psi \triangleq \psi_2 - \psi_1$ and $\Sigma\psi \triangleq \psi_2 + \psi_1$, then

$$1 + \sin\psi_1 \sin\psi_2 + \cos\psi_1 \cos\psi_2 \cos\Delta\phi = (1 + \cos\Delta\phi)\cos^2\frac{\Delta\psi}{2} + (1 - \cos\Delta\phi)\sin^2\frac{\Sigma\psi}{2} \geq 0, \quad \text{(A.8)}$$

and (A.7) becomes

$$\Sigma = 1 + \sin\psi_1 \sin\psi_2 + \cos\psi_1 \cos\psi_2 \cos\Delta\phi \quad \text{(A.9)}$$

as formulated in (7). Define also the quantity $\varepsilon \triangleq \tan^{-1}(-W_{12}/W_{11})$ that equals

$$\varepsilon = \tan^{-1}\frac{(\sin\psi_1 + \sin\psi_2)\sin\Delta\phi}{\cos\psi_1 \cos\psi_2 + (1 + \sin\psi_1 \sin\psi_2)\cos\Delta\phi}, \quad \text{(A.10)}$$

then the matrix $\mathbf{W}$ can be further generalized into

$$\mathbf{W} = \mathbf{F}_1^H\mathbf{F}_2 = \Sigma\begin{bmatrix} \cos\varepsilon & -\sin\varepsilon \\ \sin\varepsilon & \cos\varepsilon \end{bmatrix}, \quad \text{(A.11)}$$

yielding the formulas (6) and (8).

References

[1] M. Shafi, M. Zhang, A. Moustakas, P.J. Smith, A.F. Molisch, F. Tufvesson, S.H. Simon, Polarized MIMO channels in 3d: models, measurements and mutual information, IEEE J. Select. Areas Commun. 24 (2006) 514–527.

[2] R.T. Compton Jr., On the performance of a polarization sensitive adaptive array, IEEE Trans. Antennas Propagat. AP-29 (1981) 718–725.

[3] R.T. Compton Jr., The tripole antenna: an adaptive array with full polarization flexibility, IEEE Trans. Antennas Propagat. AP-29 (1981) 944–952.

[4] G.A. Deschamps, Geometrical representation of the polarization of a plane electromagnetic wave, Proc. IRE 39 (1951) 540–544.

[5] A. Nehorai, E. Paldi, Vector-sensor array processing for electromagnetic source localization, IEEE Trans. Signal Process. 42 (1994) 376–398.

[6] B. Hochwald, A. Nehorai, Polarimetric modeling and parameter estimation with applications to remote sensing, IEEE Trans. Signal Process. 43 (1995) 1923–1935.

[7] K.-C. Ho, K.-C. Tan, B.T.G. Tan, Efficient method for estimating directions-of-arrival of partially polarized signals with electromagnetic vector sensors, IEEE Trans. Signal Process. 45 (1997) 2485–2498.

[8] K.T. Wong, M.D. Zoltowski, Uni-vector-sensor ESPRIT for multisource azimuth, elevation, and polarization estimation, IEEE Trans. Antennas Propagat. 45 (1997) 1467–1474.

[9] K.T. Wong, M.D. Zoltowski, Closed-form direction finding and polarization estimation with arbitrarily spaced electromagnetic vector-sensors at unknown locations, IEEE Trans. Antennas Propagat. 48 (2000) 671–681.

[10] K.T. Wong, M.D. Zoltowski, Self-initiating MUSIC-based direction finding and polarization estimation in spatio-polarizational beamspace, IEEE Trans. Antennas Propagat. 48 (2000) 1235–1345.

[11] D. Rahamim, J. Tabrikian, R. Shavit, Source localization using vector sensor array in a multipath environment, IEEE Trans. Signal Process. 52 (2004) 3096–3103.

[12] X. Guo, S. Miron, D. Brie, Identifiability of the PARAFAC model for polarized source mixture on a vector sensor array, in: Proc. ICASSP, Las Vegas, NV, 2008, pp. 2401–2404.

[13] X. Gong, Z. Liu, Y. Xu, M.I. Ahmad, Direction-of-arrival estimation via twofold mode-projection, Signal Process. 89 (2009) 831–842.

[14] X. Guo, S. Miron, D. Brie, S. Zhu, X. Liao, A CANDECOMP/PARAFAC perspective on uniqueness of DOA estimation using a vector sensor array, IEEE Trans. Signal Process. 59 (2011) 3475–3481.

[15] A. Nehorai, M. Hawkes, Performance bounds for estimating vector systems, IEEE Trans. Signal Process. 48 (2000) 1737–1749.

[16] J. Tabrikian, R. Shavit, D. Rahamim, An efficient vector sensor conguration for source localization, IEEE Signal Processing Lett. 11 (2004) 690–693.

[17] A. Nehorai, K.-C. Ho, B.T.G. Tan, Minimum-noise-variance beamformer with an electromagnetic vector sensor, IEEE Trans. Signal Process. 47 (1999) 601–618.

[18] K.-C. Tan, K.-C. Ho, A. Nehorai, Linear independence of steering vectors of an electromagnetic vector sensor, IEEE Trans. Signal Process. 44 (1996) 3099–3107.

[19] W. Gellert, S. Gottwald, M. Hellwich, H. Kastner, H. Kunstner (Eds.), VNR Concise Encyclopedia of Mathematics, second ed., Van Nostrand Reinhold, New York, 1989, pp. 261–282.

[20] R. Bro, N.D. Sidiropoulos, G.B. Giannakis, A fast least squares algorithm for separating trilinear mixtures, in: Proc. Int. Workshop Independent Component Analysis and Blind Signal Separation, ICA'99, Aussois, France, 1999.

[21] N.D. Sidiropoulos, G.B. Giannakis, R. Bro, Blind PARAFAC receivers for DS-CDMA systems, IEEE Trans. Signal Process. 48 (2000) 810–823.

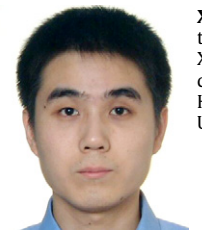

Xijing Guo received his B.Sc. degree in Information Engineering from Xi'an Jiaotong University, Xi'an, China in 2004. He is currently preparing a co-tutelle Ph.D. in signal processing at Université Henri Poincaré, Nancy, France and Xi'an Jiaotong University, Xi'an, China.

Sebastian Miron was born in Suceava, Romania, in 1977. He graduated from "Gh. Asachi" Technical University of Iasi, Romania, in 2001 and received the M.Sc. and Ph.D. degrees in signal, image, and speech processing from the Institut National Polytechnique of Grenoble, France, in 2002 and 2005, respectively.

He is currently a Maître de Conférence at Nancy-Université, France, and he is conducting research at the Centre de Recherche en Automatique de Nancy (CRAN), Nancy. His current research interests include vector-sensor array processing, positive source separation, multilinear algebra and hypercomplex numbers.

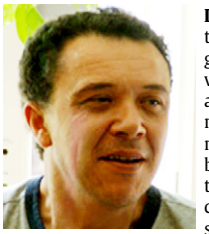

David Brie received the Ph.D. degree in 1992 and the Habilitation a' diriger des Recherches degree in 2000, both from the Henri Poincare University, Nancy, France. He is currently Professor at the telecommunication and network department from the Institut Universitaire de Technologie, Nancy-University. Since 1990, he has been with the Centre de Recherche en Automatique de Nancy. His research interests mainly concern inverse problems and multidimensional signal processing.